Published in final edited form as:

Cell Tissue Res. 2015 August ; 361(2): 427–438. doi:10.1007/s00441-015-2111-1.

Tissue underlying the intestinal epithelium elicits proliferation of intestinal stem cells following cytotoxic damage

Kristen M Seiler,
Department of Medicine and Center for Gastrointestinal Biology and Disease University of North Carolina at Chapel Hill, Chapel Hill, NC 27599, USA

Erica L Schenhals,
Department of Medicine and Center for Gastrointestinal Biology and Disease University of North Carolina at Chapel Hill, Chapel Hill, NC 27599, USA

Richard J von Furstenberg,
Department of Medicine and Center for Gastrointestinal Biology and Disease University of North Carolina at Chapel Hill, Chapel Hill, NC 27599, USA

Bhavya K Allena,
Department of Medicine and Center for Gastrointestinal Biology and Disease University of North Carolina at Chapel Hill, Chapel Hill, NC 27599, USA

Brian J Smith,
Department of Medicine and Center for Gastrointestinal Biology and Disease University of North Carolina at Chapel Hill, Chapel Hill, NC 27599, USA

Denny Scaria,
Department of Medicine and Center for Gastrointestinal Biology and Disease University of North Carolina at Chapel Hill, Chapel Hill, NC 27599, USA

Michele N Bresler,
Department of Medicine and Center for Gastrointestinal Biology and Disease University of North Carolina at Chapel Hill, Chapel Hill, NC 27599, USA

Christopher M Dekaney, and
Department of Surgery and Center for Gastrointestinal Biology and Disease University of North Carolina at Chapel Hill, Chapel Hill, NC 27599, USA

Susan J Henning
Department of Medicine and Center for Gastrointestinal Biology and Disease University of North Carolina at Chapel Hill, Chapel Hill, NC 27599, USA

Abstract

The goals of this study were to document the proliferative response of intestinal stem cells (ISCs) during regeneration after damage from doxorubicin (DXR) and to characterize the signals

Corresponding author: Susan J. Henning, Ph.D., Professor of Medicine (Gastroenterology), 4341 Medical Biomolecular Research Building (MBRB), CB# 7032, University of North Carolina at Chapel Hill, Chapel Hill, NC 27599-7032. Phone: (919) 843-4969; Fax: (919) 843-5551, sjh@med.unc.edu.

responsible for ISC activation. To this end, jejuni from DXR-treated mice were harvested for histology, assessment of ISC numbers and proliferation by flow cytometry, crypt culture, and RNA analyses. Histology showed that crypt depth and width were increased 4 days after DXR. At this time point, flow cytometry on tissue collected 1 hour after EdU administration revealed increased numbers of $CD24^{lo}UEA^{-}$ ISCs and increased percentage of ISCs cycling. In culture, crypts harvested from DXR-treated mice were equally proliferative as those of control mice. Addition of subepithelial intestinal tissue (SET) collected 4 days after DXR elicited increased budding (1.4 ± 0.3 vs. 5.1 ± 1.0 buds per enteroid). Microarray analysis of SET collected 4 days after DXR revealed 1,030 differentially expressed transcripts. Cross comparison of Gene Ontology terms considered relevant to ISC activation pointed to 10 candidate genes. Of these the epidermal growth factor (EGF) family member amphiregulin and the BMP antagonist chordin-like 2 were chosen for further study. In crypt culture, amphiregulin alone did not elicit significant budding, but amphiregulin in combination with BMP antagonism showed marked synergism (yielding 6.3 ± 0.5 buds per enteroid). These data suggest a critical role for underlying tissue in regulating ISC behavior after damage, and point to synergism between amphiregulin and chordin-like 2 as factors which may account for activation of ISCs in the regenerative phase.

Keywords

doxorubicin damage; intestinal stem cells; chordin-like 2; subepithelial tissue; amphiregulin; BMP antagonists

Introduction

Intestinal stem cells (ISCs), located in the lower portions of the crypts of Lieberkühn, are responsible not only for intestinal epithelial development and maintenance of epithelial homeostasis but also for restitution of epithelial integrity and function following damage or challenge. Current literature suggests there are two broad categories of ISCs: an actively cycling population found at the crypt base and marked by Lgr5; and one (or more) relatively quiescent population(s) located a little higher in the crypt (Barker, et al., 2012, Carlone and Breault, 2012, King and Dekaney, 2013, Potten, et al., 2009, Shaker and Rubin, 2010). The former, herein designated “active ISCs”, are believed to be primarily responsible for daily turnover of the epithelium under homeostatic conditions, whereas the latter, designated “reserve ISCs”, appear to function as a source of epithelial replacement and crypt regeneration after intestinal damage. Better understanding of factors that regulate ISC behavior will enlighten future treatment across multiple clinical scenarios. These include, but are not limited to: chemotherapy or radiation-induced mucositis, ischemia-reperfusion injury, short bowel syndrome, IBD/intestinal inflammation, intestinal polyposis syndromes, and cancer.

As has been previously reported, the commonly used chemotherapeutic agent doxorubicin (DXR) rapidly induces apoptosis in the ISC zone (Dekaney, et al., 2009, Ijiri and Potten, 1987). This causes epithelial damage including crypt loss and villus blunting, followed by epithelial regeneration (Dekaney, et al., 2009). A key component of the repair phase is restoration of crypt number, which occurs by the process of crypt fission. Prior studies

suggest that crypt fission may be driven by activation of reserve ISCs (Buczacki, et al., 2013, Dekaney, et al., 2009), however data on ISC proliferation were not provided in these reports. Thus, the first goal of our study was to use quantitative flow cytometric analysis following administration of the thymidine analog EdU to directly assess ISC proliferation following damage by DXR.

During both homeostasis and response to damage, the stem cell niche is recognized as providing key regulatory signals to the ISCs (Scoville, et al., 2008, Shaker and Rubin, 2010, Smith, et al., 2012, Tan and Barker, 2014, Yu, 2013). The niche includes epithelial elements, such as Paneth cells, which are known to secrete multiple factors capable of enhancing ISC proliferation (Clevers and Bevins, 2013), as well as subepithelial elements, such as myofibroblasts, which secrete both stimulatory and inhibitory factors (Powell, et al., 2011, Ye Lei, et al., 2014). While the complex interplay of niche components with ISCs has been widely studied following radiation damage (Yu, 2013), there is a dearth of literature on the regulation of ISC behavior following damage by chemotherapeutic drugs. This represents a major gap in current knowledge of ISCs. Therefore, our second goal was to assess the relative contributions of the crypt epithelium and the underlying tissue, hereafter referred to as sub-epithelial tissue (SET) in eliciting ISC proliferation after DXR-induced damage. We hypothesized that following cytotoxic damage, ISCs rely on signals from either the crypts themselves and/or from the SET, to proliferate and drive crypt fission, thus regenerating the epithelium. This hypothesis was tested using a crypt culture system in which crypts were grown alone or in combination with SET. Candidate ISC-regulating factors secreted by SET *in vivo* were identified by transcriptome analysis and then tested in crypt culture.

Materials and Methods

Damage and repair after DXR: animals, tissue processing, and histology

Animal experiments were performed with permission of our IACUC. Mice were housed under a 12:12-h light-dark cycle in American Association for Accreditation of Laboratory Animal Care-approved facilities. After acclimation to our facility for ≥ 1 week, 20–25 week old male C57BL/6J mice (Jackson Laboratories, Bar Harbor, HE, USA) were injected IP with DXR (15 mg/kg). Following injection, animals were provided fresh water and fed standard chow with liquid diet supplementation of Nutren 1.0 with Fiber (Nestlé Health Science, Florham Park, NJ, USA) diluted 2:1 with water. Control mice (uninjected) were maintained on this diet for an equivalent length of time. Mice were weighed daily and sacrificed at 2 day intervals, up to 8 days, after DXR injection. At sacrifice, jejunal tissue was harvested, flushed with ice-cold PBS and cut into 1cm lengths. The majority (approx. 18) of these pieces were placed into ice-cold PBS for crypt harvest and SET-co-culture (below). One piece from the mid-jejunum was incubated in zinc formalin at RT overnight, and then stored in 70% EtOH at RT until embedded in paraffin, sectioned into 5μm sections (separated by 100μm intervals) and stained with hematoxylin and eosin (H&E) for morphological assessment. Another piece from mid-jejunum was filleted open and placed into ice-cold PBS for complete epithelial dissociation to generate SET for RNA isolation. Histological measurements from H&E stained tissues were taken by a blinded scorer using Image J software (5 sections scored per biological replicate, ≥ 3 biological replicates per

time point); To quantitate crypt fission, 100 well orientated crypts were examined from each mouse. Crypt fission was defined as a bifurcating crypt with a fissure creating two (or sometimes more) flask-shaped bases with a shared single crypt-villus junction. For all histologic data, statistical comparisons of each time point with Day 0 were performed using one-way ANOVA with Tukey multiple comparison test.

Assessment of ISC cycling activity after DXR by flow cytometry

Jejunal epithelial cells were isolated from untreated and Day 4 DXR-treated mice using an EDTA/Dispase method, 1 h after IP injection of EdU (100ug/20g BW) as described previously (von Furstenberg, et al., 2011). 1 million cells from the single cell suspension were incubated in 100 μl PBS with no antibody, UEA-488 (1:500), or anti-CD24-PB (0.25μg/ml), and the EdU coupled with azide Alexa-647 dye following fixation and permeabilization using reagents and methods as reported previously (von Furstenberg, et al., 2011). Cells were analyzed by using a Beckman-Coulter CyAn ADP (Dako, Carpinteria, CA). Debris and $CD45^+$ cells were excluded based on size via bivariate plot of forward scatter (FSC) versus side scatter (von Furstenberg, et al., 2011). Doublets were excluded by successive gating on both a bivariate plot of pulse-width vs. FSC, and a bivariate plot of FSC area vs. FSC linear. Fluorescence minus one controls were used to establish gates to measure labeled cells (Roederer, 2001). Statistical comparisons of cell populations in DXR-treated vs. control mice were performed using unpaired t-tests (two-tailed).

Crypt culture

Crypts were isolated from jejuni of C57BL/6J mice via incubation in 5mM EDTA in PBS at 4°C × 30min on an orbital platform, followed by gentle hand shaking in ice-cold PBS and filtration through a 70 μm cell strainer in a manner similar to Sato et al. (Sato, et al., 2009). This crypt-enriched fraction was then pelleted by centrifugation and resuspended in hESC-qualified Matrigel (BD, San Jose, CA, USA) containing the anoikis inhibitor Y27632 (Sigma, St. Louis, MO) at a concentration of 10μM and culture factors epidermal growth factor (EGF) at 50ng/mL, noggin at 100ng/mL and R-spondin-1 at 500ng/mL, as originally reported by Sato et al. (Sato, et al., 2009) and previously described by Fuller et al. (Fuller, et al., 2013). Variations in the standard culture factors are indicated in the figure legends. Matrigel aliquots (10 μl per well containing 60–100 crypts) were plated onto 48-well culture plates (Costar, Washington, DC, USA). Plates were incubated at 37°C for 30min for Matrigel polymerization, and 200 μl per well of culture media was added containing Advanced DMEM/F12 supplemented with GlutaMAX (2mM), gentamycin/kanamycin (1:100), amphotericin B (0.25μg/mL), HEPES (10mM), N2 (1:100) and B27 (1:50). On the day of plating, the number of crypts per well was manually counted under bright field microscopy. Plates were then incubated at 37°C, and culture media was changed every 2 days, including supplementation with indicated culture factors to achieve original plating concentrations. There were ≥ 4 technical replicates per condition tested.

After 7 days in culture, the numbers of enterospheres and enteroids, as defined by the Intestinal Stem Cell Consortium (Stelzner, et al., 2012) were counted. Crypt survival per well was calculated as the total number of surviving structures (enterospheres or enteroids) divided by the original number of crypts plated in that well. The number of buds on each

surviving structure was counted under bright field microscopy. Enterospheres that survived but failed to progress to enteroids were assessed a bud number of 0. The average bud number per well was calculated as the total number of buds divided by the total number of surviving enteroids and enterospheres per well. Average bud counts from the technical replicates for each mouse were then used to calculate means ± SEM for numbers of mice (biological replicates) shown in figure legends. Statistical analysis for Fig. 3 was via unpaired *t*-tests (two-tailed).

For SET co-culture experiments, crypts were isolated from jejuni of DXR-treated mice and untreated controls, and resuspended at equal concentrations into Matrigel containing only R-spondin-1. Remnant tissue from the crypt isolation was then shaken aggressively to remove epithelium and yield SET. The SET was minced finely and added at a concentration of 1.0–1.5 μL minced SET per 50 μL Matrigel-crypt suspension prior to plating and further culture, as described above. After 7 days, bud numbers were quantified as previously described. Statistical analysis for Fig. 4 was as follows: t-test (two-tailed) was performed to compare condition A to B; paired t-tests were performed to compare condition A to C, condition A to D, and condition C to D.

In order to study the effects of amphiregulin and noggin, crypts were isolated and plated in Matrigel containing R-spondin-1, as above, in addition to either: A. no further additions; B. recombinant mouse amphiregulin (R&D, Minneapolis, MN, USA) at 100ng/mL (final concentration); C. noggin at 100ng/mL (final concentration); or D. both amphiregulin and noggin. Bud numbers were quantified after 7d in culture. Statistical analysis was performed using two-way ANOVA, with post-hoc one-way ANOVA with Tukey multiple comparison test.

To assess the potency of chordin-like 2 as compared with noggin, crypts were grown in Matrigel containing R-spondin-1 and amphiregulin as above in addition to either noggin or chordin-like 2 at concentrations of 0,10,100, or 200 ng/mL. Bud numbers were quantified after 7d in culture. Statistical analysis was performed using two-way ANOVA.

Microarray analysis, Gene Ontology and qRT-PCR

SET was stored at 4°C in RNA *later* (Qiagen, Venlo, Limburg) then removed and homogenized in a solution of 1:100 β-mercaptoethanol to Buffer RLT Plus (Qiagen, Venlo, Limburg) in Lysing Matrix tubes on a FastPrep-24 (MP biomedicals, Santa Ana, CA). Lysates were centrifuged and RNA was extracted from the supernatant using the RNeasy Plus Mini Kit (Qiagen, Venlo, Limburg). RNA from 8 biological replicates per condition (8 SET from untreated controls and 8 SET from day 4 after DXR mice) was submitted for microarray. RNA quality and concentration were assessed using a 2100 Bioanalyzer (Agilent, Santa Clara, CA, USA) and NanoDrop Spectrophotometer prior to submission to the UNC Functional Genomics Core, where total RNA (250 ng) was used to synthesize fragmented and labeled sense-strand cDNA and hybridized onto Affymetrix Mouse Gene 2.1 ST arrays (16-array plate). The Affymetrix HT WT User Manual (Santa Clara, CA, USA) was followed to prepare the samples. Partek Genomics Suite 6.6 (Partek Inc., St. Louis, MO) was used to perform data analysis. Robust multi-chip analysis (RMA) normalization was done on the entire data set. Multi-way ANOVA and fold change were

performed to select target genes that were differentially expressed between DXR SET and untreated SET. Top differentially expressed genes were selected with p value cutoff of <0.05 based on ANOVA test and 2-fold change cutoff. Hierarchical Clustering was performed on differentially expressed genes based on Average Linkage with Pearson's Dissimilarity. Gene Ontology enrichment analysis on the gene lists were performed using the Database for Annotation, Visualization and Integrated Discovery (DAVID). To determine GO term enrichment, the proportion of test genes that mapped to a particular GO term was compared with the proportion of genes from the entire GeneChip that mapped to the same term. Enriched biological process and cellular component terms shown had a p-value and FDR cutoff of <0.05. The selected regenerative candidate terms in the cross-comparison met the criteria of p-value <0.05.

To validate the microarray data and examine the time course of expression of selected transcripts in SET following DXR treatment, RNA was prepared from SET collected at day 0, 2, 4, 6, and 8 after DXR injection. For high throughput qRT-PCR, cDNA was synthesized from RNA, amplified, and included for gene expression analysis using the Fluidigm BioMark HD system according to the manufacturer's instructions (Fluidigm Corporation, South San Francisco, CA). TaqMan probes [Areg (Mm00437583_m1), Ereg (Mm00514794_m1), Tgfa (Mm00446232_m1), EGF (Mm00438696_m1)], Chrdl2 (Mm00505094_m1), Grem1 (Mm00488615_s1), and Nog (Mm01297833_s1) were obtained from Life Technologies (Grand Island, NY, USA) and used according to the manufacturer's protocol. β-Actin was used as an internal control, and fold changes were obtained using the comparative [delta][delta]Ct method. mRNA fold changes of the DXR treated groups (day 2, 4, 6, 8 following administration) were then normalized to corresponding day 0 (untreated) values, setting the control fold change to a baseline value of 1. One-way ANOVA was performed to assess statistical significance of these mRNA fold changes across the time points.

Results

The regenerative response to damage becomes evident by 4 days after DXR

As expected, treatment with DXR produced mucositis in our mice, associated with weight loss and changes in crypt number/crypt morphology. Following IP injection, the weight loss was rapid in the first 4 days, then plateaued (Fig. 1a). Crypt loss occurred, wherein the number of crypts per transverse jejunal circumference declined significantly by day 4 after DXR (Fig. 1b); this was accompanied by a decline in total jejunal circumference, though this did not reach significance (Fig. 1c). By day 4 after DXR, there was morphological evidence of crypt regeneration, with increased crypt depth (Fig. 1d), and width (Fig. 1e). This was followed by a significant increase in the rate of crypt fission at day 8 (Fig. 1f), indicating a definitive stage of damage recovery. Representative histology is shown in Fig. 1g at low power and at high power in Supplemental Fig. 1. Collectively, these data led us to further characterize events occurring at day 4 after DXR, as this seemed a likely time point in which regenerative signaling to ISCs would be strong.

ISC numbers and proliferation status are elevated 4 days after DXR

Previous work from our laboratory has shown that following staining of epithelial preparations with CD24, both ISCs and Paneth cells are found in the $CD24^{lo}$ fraction identified by flow cytometry (von Furstenberg, et al., 2011). Wong et al. subsequently demonstrated that the lectin UEA can be used to remove Paneth cells. (Wong, et al., 2012). Thus, in the current work, flow cytometry was used to exclude UEA^+ cells; the UEA^- population was then plotted as CD24 vs. EdU (to identify cycling cells). Representative flow plots are shown in Fig. 2a and the labeling strategy is shown in Fig. 2b. There was an expansion in the absolute pool of ISCs (both cycling and non-cycling): ISCs represented 4.9 ± 1.0% of all epithelial cells at day 4 after DXR vs 2.2 ± 0.6% in untreated controls (Fig. 2c). This was accompanied by increased cycling activity of ISCs at day 4 after DXR: 37 ± 6% of ISCs were cycling at this time point, as compared to 17 ± 4% in untreated controls (Fig. 2d). Interestingly, this expansion in cycling activity demonstrated a preserved ratio between cycling transit amplifying (TA) cells and cycling ISCs (Fig. 2e); 4 days after DXR 28 ± 5% of EdU^+ epithelial cells were ISCs and 72 ± 5% of EdU^+ cells were TA cells (vs. 27 ± 3% and 73 ± 3%, respectively, in untreated controls). Overall, these findings point to day 4 after DXR as a time in which ISCs were more actively cycling, and potentially responding to regenerative niche stimuli.

A minimalistic crypt culture system to study crypt responses to exogenous stimuli

In order to explore the origin of regenerative signals to the intestinal epithelium following DXR damage we needed a culture system in which crypts maintained adequate and reproducible survival, but minimal budding such that the enhanced proliferation could be easily measured. Thus, the standard culture conditions (Sato, et al., 2009) were modified as shown in Fig. 3. As can be seen, with R-spondin-1 only there was good survival after 7 days but minimal budding. Notably, there was an absolute requirement for R-spondin-1, as the absence of this factor yielded enterospheres by 24h (data not shown), but 0% survived by 7 days in culture (Fig. 3a). These data highlighted an important consideration moving forward: by minimizing buds per enteroid while maintaining a reasonable survival, minimalistic culture conditions allow easier testing of potential pro-proliferative factors.

Crypts isolated from regenerating intestine are not endogenously more proliferative

Fig. 4, panels a and b show the behavior of crypts isolated from control mice as compared with mice on day 4 following DXR. As expected, crypts harvested from untreated control mice were minimally proliferative in these culture conditions (1.4 ± 0.3 buds per enteroid). Because ISCs showed enhanced proliferation *in vivo* 4 days after DXR (Fig. 2), we hypothesized that crypts isolated from DXR-treated mice would demonstrate increased budding in culture. Surprisingly this was not observed, as crypts from these mice were also minimally proliferative (1.2 ± 0.3 buds per enteroid).

Sub-epithelial tissue isolated from regenerating intestine increases crypt budding

Fig. 4, panels c and d show the behavior of control crypts co-cultured with SET from either control mice (c) or day 4 DXR-treated mice (d). As can be seen from the comparison of panels a and c, co-culture with SET from control mice modestly enhanced proliferation as

assessed by budding behavior (1.4 ± 0.3 vs. 2.7 ± 0.2 buds per enteroid). Comparison of panels c and d shows that co-culture of SET harvested from mice 4 days after DXR yielded an additional significant increase in budding of control crypts (5.1 ± 1.0 buds per enteroid). This suggested that SET releases stimuli which induce epithelial proliferation, and that these signals are heightened during repair from cytotoxic injury.

Transcriptome analysis reveals regenerative signals originating from SET after damage

Microarray analysis performed on RNA extracted from SET harvested from mice 4 days after DXR as compared to untreated controls revealed 1030 differentially regulated genes (listed in Supplemental Table 1). Hierarchical clustering showed clear distinctions between treatment groups (Fig. 5). Overall GO analysis of biological processes (Fig. 6a) showed enrichment for transcripts expected to be associated with response to damage (e.g. “response to stimulus”, “response to stress”, etc.) and immune infiltration (“inflammatory response”) as well as those associated with repair (e.g. “cell cycle”, “M phase”, etc.). Within the cellular component arm of GO, the 2 most abundant categories were “extracellular region” and “extracellular space” (Fig. 6b), consistent with SET being highly secretory, as already deduced from the co-culture experiment. In order to identify specific candidate genes, the GO terms “binding,” “extracellular region,” and “tissue development” were considered relevant to ISC activation. As can be seen in Fig. 6c, when these were combined a total of 10 genes emerged. Of these (shown in Fig. 6d), the most up-regulated was the EGF family member amphiregulin, (7.53 fold enriched) and the third highest was the BMP antagonist chordin-like 2 (4.5 fold enriched). Given the growing body of literature implicating amphiregulin in intestinal epithelial regulation (Hitch, et al., 2012, Shao and Sheng, 2010), and mounting evidence that ErbB receptor status may regulate ISC activation (Powell, et al., 2012, Wong, et al., 2012), we selected amphiregulin as an attractive candidate to test in culture for its ability to elicit crypt proliferation. Further, in view of the elevated expression of chordin-like 2, we explored the potential beneficial role of concomitant BMP antagonism.

Amphiregulin increases crypt budding *in vitro* provided BMP signaling is inhibited

To assess the proliferative capacity of amphiregulin in our enteroid culture system, crypts were grown under minimal conditions (as in Fig. 3) with the addition of either amphiregulin alone or amphiregulin in combination with noggin which is the standard BMP antagonist traditionally used in enteroid cultures (Sato and Clevers, 2013). Despite the fact that amphiregulin transcripts were 7.5 fold increased in SET harvested 4 days after DXR (Fig. 6), the culture data shown in Fig. 7 (panels a versus b) show that recombinant amphiregulin alone does not recapitulate the stimulatory effect of Day 4 SET observed in Fig. 4. Likewise, despite the 4.5 fold increase in chordin-like 2 expression, inhibition of BMP signaling via the analogous antagonist noggin was insufficient to elicit crypt budding (Fig. 7, panels c versus a). However in the presence of amphiregulin and noggin there was a dramatic stimulation of the crypts, with average bud numbers (6.3 ± 0.5 buds per enteroid) mirroring those seen with Day 4 SET (Fig. 4). Not only did the one-way ANOVA show significance of the combination treatment (Fig. 7 panel d versus c), but the two-way ANOVA showed a highly significant interaction of amphiregulin and noggin ($p<0.001$), thus documenting the obvious synergism between these two factors.

In biochemical studies noggin and chordin-like 2 have been shown to have equivalent potencies for inhibition of purified BMP4 (Nakayama, et al., 2004) which is the principal BMP found in the tissue underlying intestinal crypts (Haramis, et al., 2004, He, et al., 2004). However, the influence of chordin-like 2 has not been previously studied in the intestinal epithelium. Thus, after observing the importance of BMP antagonism using noggin in Fig. 7, we directly compared the potency of these two BMP antagonists as facilitators of the proliferative response to amphiregulin. As can be seen in Fig. 8, the dose response of crypt budding was very similar using chordin-like 2 as compared with noggin. This indicates that elevated expression of chordin-like 2 in SET *in vivo* is likely to have a functional role in the regenerative response to DXR.

Time course of elevated expression of amphiregulin and chordin-like 2

In order to more carefully assess the potential roles of amphiregulin and chordin-like 2 in the regenerative response *in vivo*, we used quantitative RT-PCR to examine the time course of elevated expression of these factors and their family members. As can be seen in Fig. 9a, amphiregulin mRNA was rapidly induced, peaking at Day 2 after DXR. Transcripts of two other EGF family members, namely epiregulin and transforming growth factor α (TGFα), were also significantly elevated with a similar time course, but to only modest levels when compared with amphiregulin. Interestingly, EGF mRNA levels in the SET showed no significant change following DXR treatment. All three BMP antagonists examined (Fig. 9b) showed induction in response to DXR with a slower time course than the EGF family. Of the three, chordin-like 2 is clearly the dominant transcript with increases exceeding 25-fold at Day 4 and exceeding 100-fold at Day 6.

Discussion

The primary goal of this study was to characterize the role of the ISC niche in eliciting epithelial repair after damage from DXR. To this end, we initially determined a time point—day 4 after DXR—in which regenerative signaling was likely to be strong. Next, we demonstrated increased ISC numbers and proliferation at this time, with a concomitant proportional increase in transit amplifying cell proliferation. We then used tightly controlled crypt culture conditions to show that crypts isolated from regenerating tissue (day 4 after DXR) were not inherently more proliferative, but that SET isolated from regenerating tissue was capable of enhancing enteroid budding. Transcriptome analysis of SET revealed candidate factors that may control epithelial responses to damage. Two of these factors, amphiregulin and chordin-like 2, were tested in culture and were shown to have a dramatic combined effect on crypt expansion.

Although previous work has demonstrated increased epithelial proliferation after DXR (Dekaney, et al., 2009), the focus of the current study was specifically on the ISC fraction of the epithelium. Our quantitative flow cytometric analysis with anti-CD24 and UEA showed greater than 2-fold increases in both the number of ISCs and the proportion of the ISC pool that were actively cycling. While there have been extensive studies on the responses of ISCs following radiation (Hua, et al., 2012, May, et al., 2008, Metcalfe, et al., 2014, Potten, 2004, Powell, et al., 2012, Van Landeghem, et al., 2012, Yan, et al., 2012, Yu, 2013), our work

constitutes the first detailed report of ISC behavior following DXR damage. Interestingly, two prior studies had pointed to the possibility that the reserve ISC fraction is activated in the regenerative phase after DXR treatment. First, Dekaney et al. reported increased numbers of side population cells (Dekaney, et al., 2009) that have subsequently been shown to be non-cycling under homeostatic conditions (von Furstenberg, et al., 2013). However, proliferation of this population in response to DXR has not been investigated. The other published study of ISCs after DXR is that by Buczacki et al. which reported lineage tracing from the label-retaining reserve ISC pool (Buczacki, et al., 2013). While this implies proliferation, no quantitative data were provided (in fact only a single positive mouse was reported). In our work, the $CD24^{lo}$ fraction appears to include both active and reserve ISC populations (Buczacki, et al., 2013, von Furstenberg, et al., 2011). As such, the increased EdU incorporation at day 4 after DXR likely represents both activation of the reserve ISCs and increased proliferation of the active ISC population. Interestingly, we found that the ratio of cycling ISCs to cycling TA cells was maintained between day 4 after DXR and untreated conditions. This suggests tight biological regulation, and merits further investigation into mechanisms that control this proportional expansion.

In order to assess the role of epithelial versus stromal factors in eliciting proliferation of ISCs after DXR damage, we turned to an *in vitro* approach. In recent years, Matrigel- based ISC and intestinal crypt cultures have emerged as powerful techniques with which to study ISC behavior *ex vivo* (Leushacke and Barker, 2014, Sato and Clevers, 2013, Sato, et al., 2009), in the absence of the complex and intertwined forces at play *in vivo*. In such cultures, crypts initially form enterospheres that progress to budding structures termed enteroids (Stelzner, et al., 2012). Bud number has been established as a reliable and reproducible method of assessing crypt proliferation in culture (Fuller, et al., 2012). While traditional crypt cultures have multiple factors designed to optimize proliferation, for the current work we needed to minimize proliferation in order to observe the hypothesized enhancement of proliferation with tissues from DXR-treated mice. Similar to the report by Chen et al. using crypts from the distal intestine (Chen, et al., 2012), in our jejunal crypt cultures we found that in lieu of the standard combination of EGF, noggin and R-spondin-1, R-spondin-1 alone allowed survival but minimal budding.

Using these conditions, despite *in vivo* evidence of increased epithelial and ISC proliferation during repair from DXR-induced epithelial damage, we observed no difference in endogenous *in vitro* proliferative capacity of crypts isolated from mice before vs. after DXR damage (Fig. 4). However, the addition of SET from recovering intestine yielded a significant increase in enteroid budding, suggesting that regenerative stimuli may originate from below the epithelium. Although we have not identified which cells within the SET survive over the 7 days of incubation, prior studies have demonstrated that myofibroblasts can grow in these Matrigel cultures (Kabiri, et al., 2014, Ye Lei, et al., 2014). As discussed below, myofibroblasts are a likely source of the two prime candidates for eliciting crypt budding. To put the co-culture data in the appropriate context, a key point is that each enteroid bud typically has all the features of a new crypt (Sato, et al., 2009). Thus, we believe the process of budding is the *in vitro* approximate of *in vivo* crypt fission, which is a critical component of repair after damage (Wright, 2000). Moreover, since crypt fission is

believed to be driven by a doubling of the number of ISCs (Totafurno, et al., 1987), our observed SET effect suggests that by day 4 after DXR, stromal elements are secreting factors which enhance ISC proliferation.

Microarray analysis of the SET (Figs 5 and 6) revealed two attractive candidate factors that may contribute to ISC proliferation after damage. amphiregulin, a member of the EGF family of proteins, is known to be pro-proliferative and to play a central role in repair and branching morphogenesis in various tissues (Berasain and Avila, 2014). On the other hand chordin-like 2 is a BMP antagonist (Nakayama, et al., 2004) and thus would be expected to have a permissive effect on proliferation by blocking the inhibitory actions of BMP signaling. Prior studies in the intestine demonstrated upregulation of amphiregulin during regeneration after whole body irradiation, where amphiregulin production was localized to intestinal sub-epithelial myofibroblasts (Shao and Sheng, 2010). Further, using amphiregulin knockout mice, it was shown that crypt proliferation was unaltered in amphiregulin −/− mice at baseline but significantly hindered following irradiation, highlighting the importance of this molecule, specifically in the context of damage response. Chordin-like 2 has not been previously reported in the small intestine. However, other BMP antagonists, namely gremlin1, gremlin2, and chordin-like 1 have been shown to be produced by myofibroblasts at the bases of colonic crypts, where they are thought to enhance proliferation of epithelial cells, including stem cells, in that location (Kosinski, et al., 2007, Powell, et al., 2011). In addition, over-expression of noggin, another member of the BMP antagonist family, can lead to both crypt fission (Batts, et al., 2006) and *de novo* crypt formation (Haramis, et al., 2004). The same outcomes are observed when BMP signaling is blocked by ablation of BMP receptors (Auclair, et al., 2007, He, et al., 2004).

Based on this literature, we expected amphiregulin to increase proliferative activity of jejunal crypts *in vitro* and for BMP antagonism to possibly enhance this effect. Interestingly, under the culture conditions used (Fig. 7), addition of recombinant amphiregulin alone did not increase enteroid budding. However, in the presence of both amphiregulin and BMP antagonism (using either noggin or chordin-like 2), there was dramatic stimulation, yielding bud numbers equivalent to those seen during co-culture with SET isolated 4 days after DXR (Fig. 4). The fact that the proliferative effect of amphiregulin only became apparent when BMP signaling was inhibited, implies presence of BMPs in this culture system. Since stromal elements, which are the usual source of BMPs *in vivo* (Haramis, et al., 2004, He, et al., 2004), were not included in the study shown in Fig. 7, the most likely source of BMPs is the Matrigel (Paralkar, et al., 1992). In intact tissue, endogenous BMPs in the lamina propria would play an analogous role. Thus, we propose that the increases in expression of amphiregulin and chordin-like 2 observed in SET *in vivo* are responsible for the increased ISC proliferation observed at day 4 after DXR. Confirmation of this suggestion will require demonstration that pharmacologic or genetic ablation of amphiregulin or chordin-like 2 prevents the ISC regenerative response following DXR. Such studies are a logical future direction.

Our qRT-PCR study revealed some interesting nuances (Fig. 9). First, within the EGF family, two other members, namely epiregulin and TGFα, were up-regulated following DXR. Transcript levels of all three EGF family members peaked at Day 2 and remained

elevated at Day 4. However, at both these time points it was clear that amphiregulin was the dominant mRNA, with induced levels being 5–6-fold and 9–12-fold higher than those of epiregulin and TGFα, respectively. Likewise, although statistical analyses indicated that the three BMP antagonists (chordin-like 2, gremlin 1, and noggin) were all up-regulated in response to DXR damage, only chordin-like 2 displayed a robust increase likely to have biological significance. Taken together, our findings point to a novel mechanism that may be critical for repair of the intestinal epithelium following various insults. Further, our demonstration of the potent synergism between amphiregulin and BMP antagonism in stimulation of enteroid budding *in vitro*, suggests that *in vivo* these two pathways may provide the driving force for ISC activation and, subsequently, restoration of crypt number via crypt fission. The fact that the surge of chordin-like 2 expression was delayed as compared with that of amphiregulin suggests continued BMP antagonism may be important in allowing the progression from ISC activation to crypt fission. Further studies to elucidate the cellular and molecular biology of these processes are clearly warranted, and have obvious translational applications.

While our transcript analyses of SET following DXR led us to focus on two families of factors that are likely secreted by myofibroblasts, we recognize that the cellular response to the DXR damage is complex. For example, one cannot overlook the importance of the inflammatory reaction elicited by epithelial compromise, and the role that immune cells play in orchestrating tissue responses. Indeed, blinded scoring of tissue sections following DXR revealed an acute inflammatory response (see high power images in Supplemental Fig. 1). The possibility that these immune cells influence ISC behavior, either by direct signaling to ISCs, or by indirect signaling though myofibroblasts or other cell types, deserves further attention, but was beyond the scope of the current study.

Looking to the future, our current findings, together with previous work that has pointed to reserve ISCs as being the regenerative source of new crypts, suggest two translational applications. The first is the combined delivery of an EGF family member with a BMP antagonist to accelerate the *in vivo* activation of reserve ISCs following intestinal damage, thus limiting the extent and duration of epithelial compromise. The second is the use of similar combinations of these factors to propagate reserve ISCs *in vitro* for use in transplantation. To date, ISC culture protocols have been optimized for expansion of the active subpopulation of ISCs. While reserve ISCs typically grow under these conditions, their biology may be abnormal. Thus, full exploration of the signaling pathways operative *in vivo*, and application of these to generate culture conditions that preserve normal behavior of the reserve ISC fraction, may be of significant value to the field of tissue engineering.

Supplementary Material

Refer to Web version on PubMed Central for supplementary material.

Acknowledgments

Funding

This work was supported by the National Institutes of Health (NIH) Grants P30 DK034987, and U01-DK085547. The latter grant is part of the Intestinal Stem Cell Consortium, a collaborative research project funded by the National Institute of Diabetes and Digestive and Kidney Diseases (NIDDK) and the National Institute of Allergy and Infectious Diseases. Kristen Seiler was supported by the Medical Student Research Training Program (MSRTP) from the NIDDK funded as a supplement to NIH grant T32-DK007737. The UNC Flow Cytometry Core Facility is supported in part by NCI Center Core Support Grant (P30 CA016086) to the UNC Lineberger Comprehensive Cancer Center.

We wish to thank: Ajay Gulati, MD and Richard Moffitt, PhD for their input toward experimental design of this project; Allison Rogala, DVM for histologic assessment of inflammation in DXR-treated intestinal tissue; and Carlton W. Anderson and Scott T. Magness, PhD of the Center for Gastrointestinal Biology and Disease's Advanced Analytics Core for their valuable technical assistance with the Fluidigm qRT-PCR. We additionally acknowledge Joe Galanko, PhD for statistical advice, Marcus Muehlbauer, MD PhD for constructive input on the revised manuscript, Carolyn Suitt (UNC CGIBD Histology Core), Mike Vernon (UNC Functional Genomics Core) and valuable assistance from the UNC Flow Cytometry Core.

References

Auclair BA, Benoit YD, Rivard N, Mishina Y, Perreault N. Bone morphogenetic protein signaling is essential for terminal differentiation of the intestinal secretory cell lineage. Gastroenterology. 2007; 133:887–896. [PubMed: 17678919]

Barker N, van Oudenaarden A, Clevers H. Identifying the stem cell of the intestinal crypt: strategies and pitfalls. Cell Stem Cell. 2012; 11:452–460. [PubMed: 23040474]

Batts LE, Polk DB, Dubois RN, Kulessa H. BMP signaling is required for intestinal growth and morphogenesis. Dev Dyn. 2006; 235:1563–1570. [PubMed: 16538672]

Berasain C, Avila MA. Amphiregulin. Semin Cell Dev Biol. 2014; 23:00006–00008.

Buczacki SJ, Zecchini HI, Nicholson AM, Russell R, Vermeulen L, Kemp R, Winton DJ. Intestinal label-retaining cells are secretory precursors expressing Lgr5. Nature. 2013; 495:65–69. [PubMed: 23446353]

Carlone DL, Breault DT. Tales from the crypt: the expanding role of slow cycling intestinal stem cells. Cell Stem Cell. 2012; 10:2–4. [PubMed: 22226346]

Chen CL, Yu X, James IO, Zhang HY, Yang J, Radulescu A, Zhou Y, Besner GE. Heparin-binding EGF-like growth factor protects intestinal stem cells from injury in a rat model of necrotizing enterocolitis. Lab Invest. 2012; 92:331–344. [PubMed: 22157721]

Clevers H, Bevins C. Paneth Cells: Maestros of the Small Intestinal Crypts. Annual Review of Physiology. 2013; 75:289–311.

Dekaney CM, Gulati AS, Garrison AP, Helmrath MA, Henning SJ. Regeneration of intestinal stem/progenitor cells following doxorubicin treatment of mice. American Journal of Physiology-Gastrointestinal and Liver Physiology. 2009; 297:G461–G470. [PubMed: 19589945]

Fuller MK, DMF, Sundaram N, Mahe MM, Stout KM, Furstenberg RJv, Smith BJ, McNaughton KK, Shroyer NF, Helmrath MA, Henning SJ. Intestinal stem cells remain viable after prolonged tissue storage. Cell and Tissue Research. 2013; 354:441–450. [PubMed: 23820734]

Fuller MK, Faulk DM, Sundaram N, Shroyer NF, Henning SJ, Helmrath MA. Intestinal crypts reproducibly expand in culture. The Journal of surgical research. 2012; 178:48–54. [PubMed: 22564827]

Haramis AP, Begthel H, van den BM, van Es J, Jonkheer S, Offerhaus GJ, Clevers H. De novo crypt formation and juvenile polyposis on BMP inhibition in mouse intestine. Science. 2004; 303:1684–1686. [PubMed: 15017003]

He XC, Zhang J, Tong WG, Tawfik O, Ross J, Scoville DH, Tian Q, Zeng X, He X, Wiedemann LM, Mishina Y, Li L. BMP signaling inhibits intestinal stem cell self-renewal through suppression of Wnt-beta-catenin signaling. Nature Genetics. 2004; 36:1117–1121. [PubMed: 15378062]

Hitch MC, Leinicke JA, Wakeman D, Guo J, Erwin CR, Rowland KJ, Merrick EC, Heuckeroth RO, Warner BW. Ret heterozygous mice have enhanced intestinal adaptation after massive small bowel resection. American Journal of Physiology-Gastrointestinal and Liver Physiology. 2012; 302:G1143–1150. [PubMed: 22421622]

Hua G, Thin TH, Feldman R, Haimovitz-Friedman A, Clevers H, Fuks Z, Kolesnick R. Crypt base columnar stem cells in small intestines of mice are radioresistant. Gastroenterology. 2012; 143:1266–1276. [PubMed: 22841781]

Ijiri K, Potten CS. Further studies on the response of intestinal crypt cells of different hierarchical status to eighteen different cytotoxic agents. Br J Cancer. 1987; 55:113–123. [PubMed: 3814484]

Kabiri Z, Greicius G, Madan B, Biechele S, Zhong Z, Zaribafzadeh H, Edison, Aliyev J, Wu Y, Bunte R, Williams BO, Rossant J, Virshup DM. Stroma provides an intestinal stem cell niche in the absence of epithelial Wnts. Development (Cambridge, England). 2014; 141:2206–2215.

King SL, Dekaney CM. Small intestinal stem cells. Curr Opin Gastroenterol. 2013; 29:140–145. [PubMed: 23380573]

Kosinski C, Li VS, Chan AS, Zhang J, Ho C, Tsui WY, Chan TL, Mifflin RC, Powell DW, Yuen ST, Leung SY, Chen X. Gene expression patterns of human colon tops and basal crypts and BMP antagonists as intestinal stem cell niche factors. Proc Natl Acad Sci USA. 2007; 104:15418–15423. [PubMed: 17881565]

Leushacke M, Barker N. Ex vivo culture of the intestinal epithelium: strategies and applications. Gut. 2014; 63:1345–1354. [PubMed: 24841573]

May R, Riehl TE, Hunt C, Sureban SM, Anant S, Houchen CW. Identification of a novel putative gastrointestinal stem cell and adenoma stem cell marker, doublecortin and CaM kinase-like-1, following radiation injury and in adenomatous polyposis coli/multiple intestinal neoplasia mice. Stem Cells. 2008; 26:630–637. [PubMed: 18055444]

Metcalfe C, Kljavin N, Ybarra R, de Sauvage F. Lgr5+ Stem Cells Are Indispensable for Radiation-Induced Intestinal Regeneration. Cell Stem Cell. 2014; 14:1–11. [PubMed: 24388168]

Nakayama N, Han CY, Cam L, Lee JI, Pretorius J, Fisher S, Rosenfeld R, Scully S, Nishinakamura R, Duryea D, Van G, Bolon B, Yokota T, Zhang K. A novel chordin-like BMP inhibitor, CHL2, expressed preferentially in chondrocytes of developing cartilage and osteoarthritic joint cartilage. Development (Cambridge, England). 2004; 131:229–240.

Paralkar V, Weeks B, Yu Y, Kleinman H, Reddi A. Recombinant Human Bone Morphogenetic Protein 2B Stimulates PC12 Cell Differentiation: Potentation and Binding to Type IV Collagen. The Journal of Cell Biology. 1992; 119:1721–1728. [PubMed: 1469059]

Potten CS. Radiation, the ideal cytotoxic agent for studying the cell biology of tissues such as the small intestine. Radiat Res. 2004; 161:123–136. [PubMed: 14731078]

Potten CS, Gandara R, Mahida YR, Loeffler M, Wright NA. The stem cells of small intestinal crypts: where are they? Cell Proliferation. 2009; 42:731–750. [PubMed: 19788585]

Powell AE, Wang Y, Li Y, Poulin EJ, Means AL, Washington MK, Higginbotham JN, Juchheim A, Prasad N, Levy SE, Guo Y, Shyr Y, Aronow BJ, Haigis KM, Franklin JL, Coffey RJ. The pan-ErbB negative regulator Lrig1 is an intestinal stem cell marker that functions as a tumor suppressor. Cell. 2012; 149:146–158. [PubMed: 22464327]

Powell DW, Pinchuk IV, Saada JI, Chen X, Mifflin RC. Mesenchymal cells of the intestinal lamina propria. Annu Rev Physiol. 2011; 73:213–237. [PubMed: 21054163]

Roederer M. Spectral compensation for flow cytometry: visualization artifacts, limitations, and caveats. Cytometry. 2001; 45:194–205. [PubMed: 11746088]

Sato T, Clevers H. Primary mouse small intestinal epithelial cell cultures. Methods Mol Biol. 2013; 945:319–328. [PubMed: 23097115]

Sato T, Vries RG, Snippert HJ, van de WM, Barker N, Stange DE, van Es JH, Abo A, Kujala P, Peters PJ, Clevers H. Single Lgr5 stem cells build crypt-villus structures in vitro without a mesenchymal niche. Nature. 2009; 459:262–265. [PubMed: 19329995]

Scoville DH, Sato T, He XC, Li L. Current view: intestinal stem cells and signaling. Gastroenterology. 2008; 134:849–864. [PubMed: 18325394]

Shaker A, Rubin DC. Intestinal stem cells and epithelial-mesenchymal interactions in the crypt and stem cell niche. Transl Res. 2010; 156:180–187. [PubMed: 20801415]

Shao J, Sheng H. Amphiregulin promotes intestinal epithelial regeneration: roles of intestinal subepithelial myofibroblasts. Endocrinology. 2010; 151:3728–3737. [PubMed: 20534719]

Smith N, Davies P, Silk A, Wong M. Epithelial and Mesenchymal Contribution to the Niche: A Safeguard for Intestinal Stem Cell Homeostasis. Gastroenterology. 2012; 143:1426–1430. [PubMed: 23085353]

Stelzner M, Helmrath M, Dunn JCY, Henning SJ, Houchen CW, Kuo C, Lynch J, Li L, Magness ST, Martin MG, Wong MH, Yu J. A nomenclature for intestinal in vitro cultures. American Journal of Physiology-Gastrointestinal and Liver Physiology. 2012; 302:1359–1363.

Tan D, Barker N. Intestinal Stem Cells and Their Defining Niche. Current Topics in Developmental Biology. 2014; 107:77–107. [PubMed: 24439803]

Totafurno J, Bjerknes M, Cheng H. The Crypt Cycle. Crypt and villus production in the adult intestinal epithelium. Biophysiology Journal. 1987; 52:279–294.

Van Landeghem L, Santoro MA, Krebs AE, Mah AT, Dehmer JJ, Gracz AD, Scull BP, McNaughton K, Magness ST, Lund PK. Activation of two distinct Sox9-EGFP-expressing intestinal stem cell populations during crypt regeneration after irradiation. American Journal of Physiology-Gastrointestinal and Liver Physiology. 2012; 302:1111–1132.

von Furstenberg RJ, Buczacki SJ, Smith BJ, Seiler KM, Winton DJ, Henning SJ. Side population sorting separates subfractions of cycling and non-cycling intestinal stem cells. Stem Cell Res. 2013; 12:364–375. [PubMed: 24365601]

von Furstenberg RJ, Gulati AS, Baxi A, Doherty JM, Stappenbeck TS, Gracz AD, Magness ST, Henning SJ. Sorting mouse jejunal epithelial cells with CD24 yields a population with characteristics of intestinal stem cells. American Journal of Physiology-Gastrointestinal and Liver Physiology. 2011; 300:G409–G417. [PubMed: 21183658]

Wong VWY, Stange DE, Page ME, Buczacki S, Wabik A, Itami S, van de Wetering M, Poulsom R, Wright NA, Trotter MWB, Watt FM, Winton DJ, Clevers H, Jensen KB. Lrig1 controls intestinal stem-cell homeostasis by negative regulation of ErbB signalling. Nat Cell Biol. 2012; 14:401–408. [PubMed: 22388892]

Wright NA. Epithelial stem cell repertoire in the gut: clues to the origin of cell lineages, proliferative units and cancer. Int J Exp Pathol. 2000; 81:117–143. [PubMed: 10762441]

Yan KS, Chia LA, Li X, Ootani A, Su J, Lee JY, Su N, Luo Y, Heilshorn SC, Amieva MR, Sangiorgi E, Capecchi MR, Kuo CJ. The intestinal stem cell markers Bmi1 and Lgr5 identify two functionally distinct populations. Proc Natl Acad Sci U S A. 2012; 109:466–471. [PubMed: 22190486]

Ye Lei N, Jabaji Z, Wang J, Joshi V, Brinkley G, Khalil H, Wang F, Jaroszewicz A, Pellegrini M, Li L, Lewis M, Stelzner M, Dunn J, Martin M. Intestinal Subepithelial Myofibroblasts Support the Growth of Intestinal Epithelial Stem Cells. PLoS One. 2014; 9:e84651. [PubMed: 24400106]

Yu J. Intestinal stem cell injury and protection during cancer therapy. Transl Cancer Res. 2013; 2:384–396. [PubMed: 24683536]

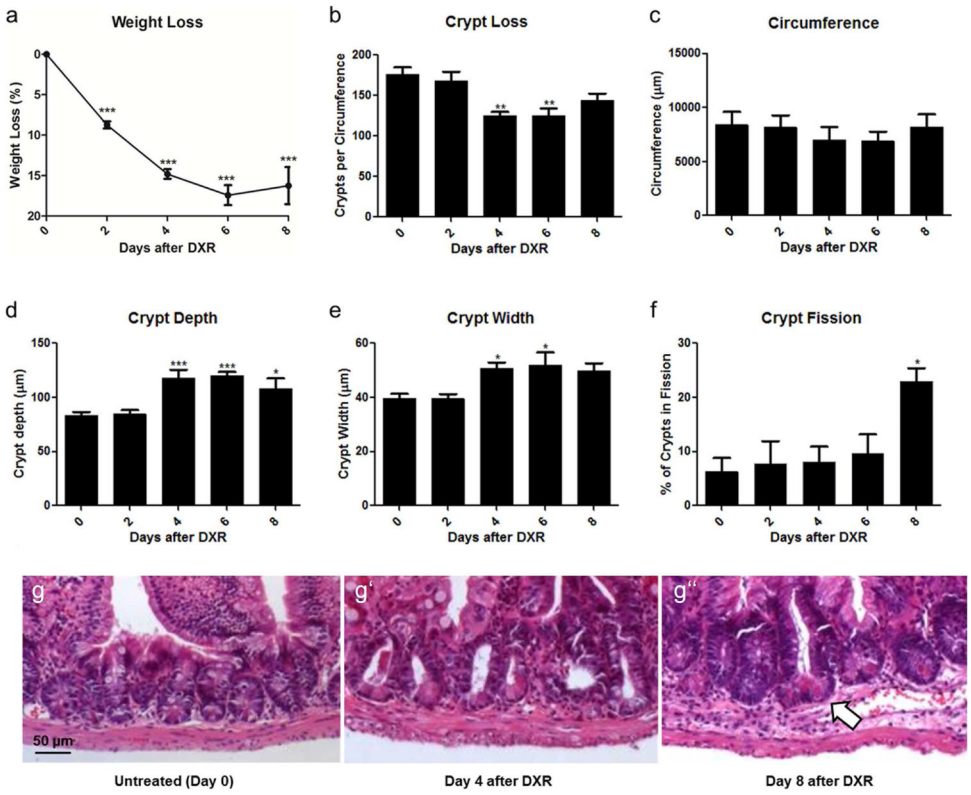

Fig. 1.

Damage and repair of jejunum after doxorubicin (DXR**). a**: Animal weight loss after IP injection of DXR, where Day 0 represents the reference point for each mouse before DXR injection. **b–f**: Quantitative analysis of crypt number, jejunal circumference, crypt depth, crypt width, and crypt fission over time after DXR, with data at Days 2, 4, 6 and 8 showing DXR-injected mice and Day 0 showing control uninjected mice. **g**: Representative images of crypt morphology (10x), with scale bar equivalent to 50µm and with crypt fission denoted by the white arrow. Bar graphs plotted as mean ± SEM ($n \geq 3$ for each time point). Asterisks show comparison with day 0 (i.e. no DXR). *p <0.05, **p <0.01, ***p <0.001.

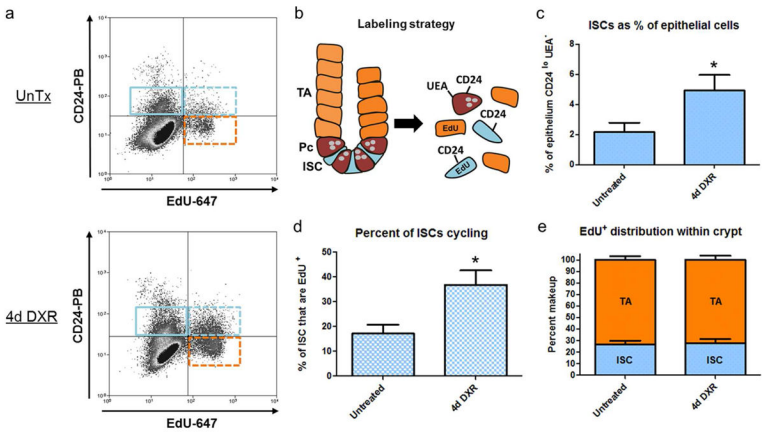

Fig. 2.

Intestinal stem cell (ISC) numbers and proliferation status are elevated 4 days after doxorubicin (DXR). **a**: Flow cytometry was used to identify non-cycling ISCs ($CD24^{lo}$/UEA^{-}/EdU^{-}) denoted by solid blue gate, cycling ISCs ($CD24^{lo}$/UEA^{-}/EdU^{+}) dashed blue gate, and cycling transit amplifying cells (UEA^{-}/$CD24^{-}$/Edu^{+}) dashed orange gate. Cells displayed in this panel were depleted of UEA^{+} cells in prior gate (not shown), **b**: Marker strategy used for identification of total ISCs, cycling ISCs, and (TA) cells, **c**: The contribution of ISCs as a percent of total epithelium before (n=6) and 4 days after DXR (n=7), **d**: Percent of ISCs cycling before and after DXR, **e**: The ratio of ISCs to transit amplifying cells before and after DXR. Bar graphs plotted as mean ± SEM. *p <0.05. TA-Transit Amplifying; Pc- Paneth cell

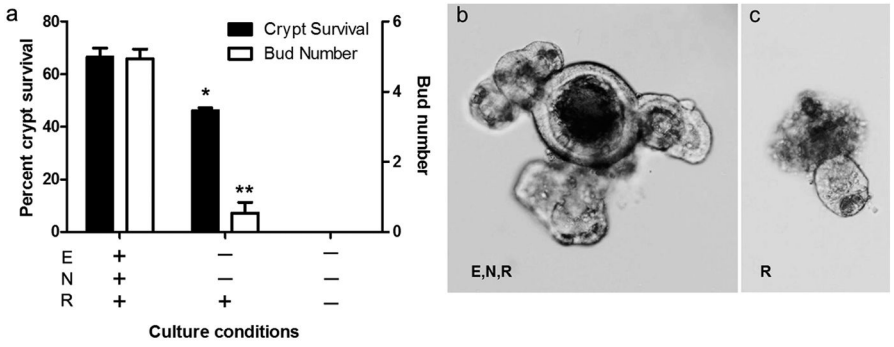

Fig. 3.

Establishing minimal crypt culture conditions. **a**: The effect of different conditions on crypt survival over 7d (solid bars) and on bud number per enteroid at 7d (open bars); **b**,**c**: Representative images of crypt progression after 7d in culture under routine Sato conditions (ENR) vs. R alone (10x). Bar graphs plotted as mean ± SEM (n=2–3). Asterisks show comparison with ENR. *p <0.05. **p<0.01. E- Epidermal Growth Factor; N- noggin; R- R-spondin-1

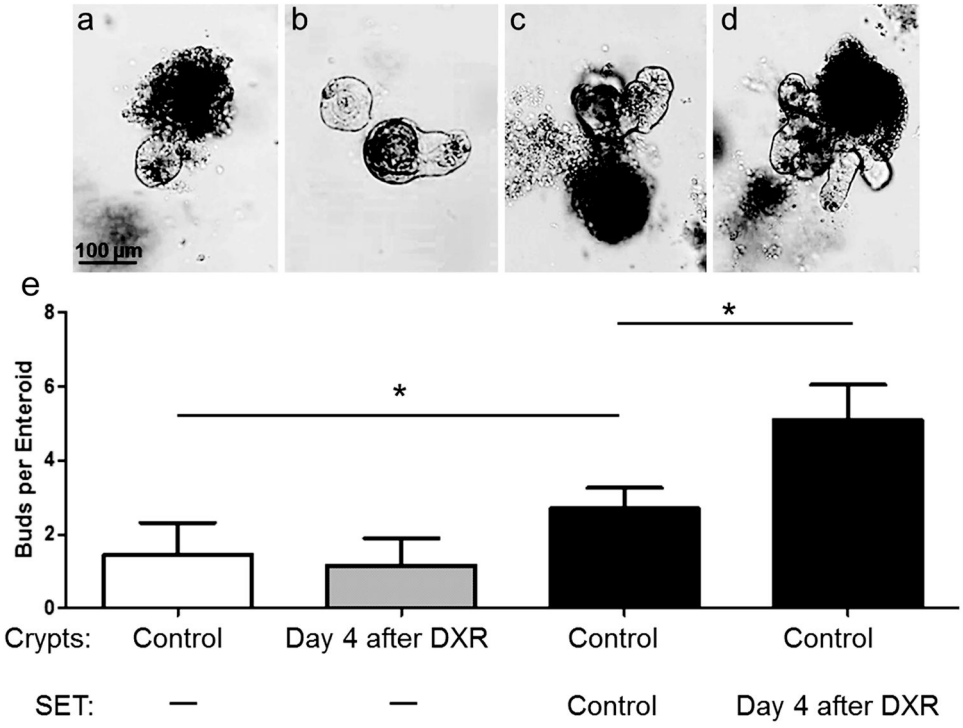

Fig. 4.

Endogenous proliferation of crypts, and the effect of sub-epithelial tissue (SET) on crypt budding. The average bud number of crypts after 1 week in culture is shown across 4 culture conditions, with representative images: **a**: Control (untreated) crypts (n=8), **b**: Day 4 after doxorubicin (DXR) crypts (n=7), **c**: Co-culture of control crypts + control SET (n=8), **d**: Co-culture of control crypts + day 4 after DXR SET (n=7). All images 10X with bar showing 100 µm. Graphs plotted as mean ± SEM. *p<0.05.

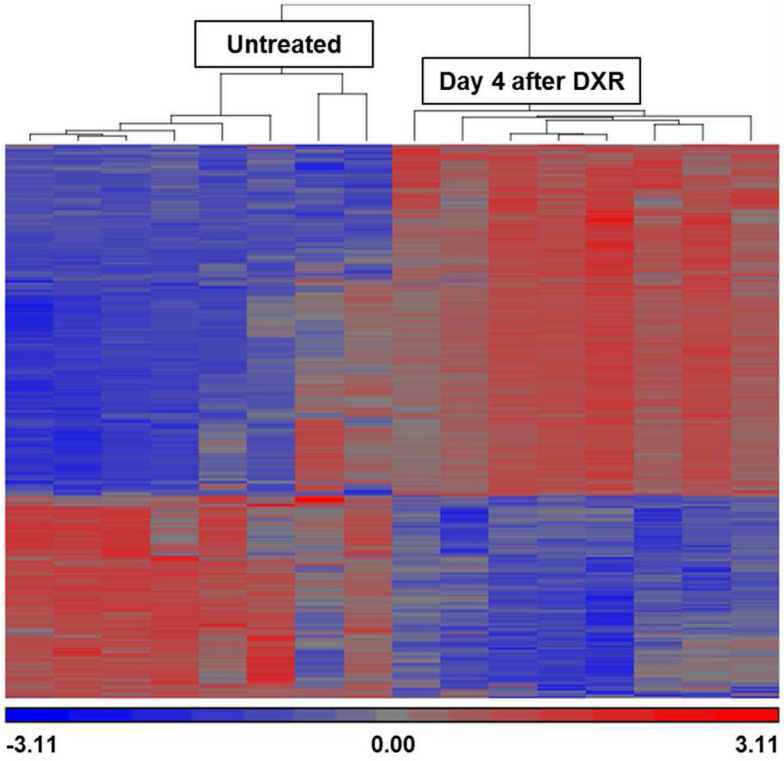

Fig. 5.

Microarray analysis of sub-epithelial tissue (SET). Microarray heat map of SET from untreated control mice (n=8) vs. SET from mice on day 4 after doxorubicin (DXR) (n=8). Each lane represents an individual mouse and results of hierarchical clustering are shown above the lanes. Upregulated and downregulated genes are indicated by red and blue, respectively.

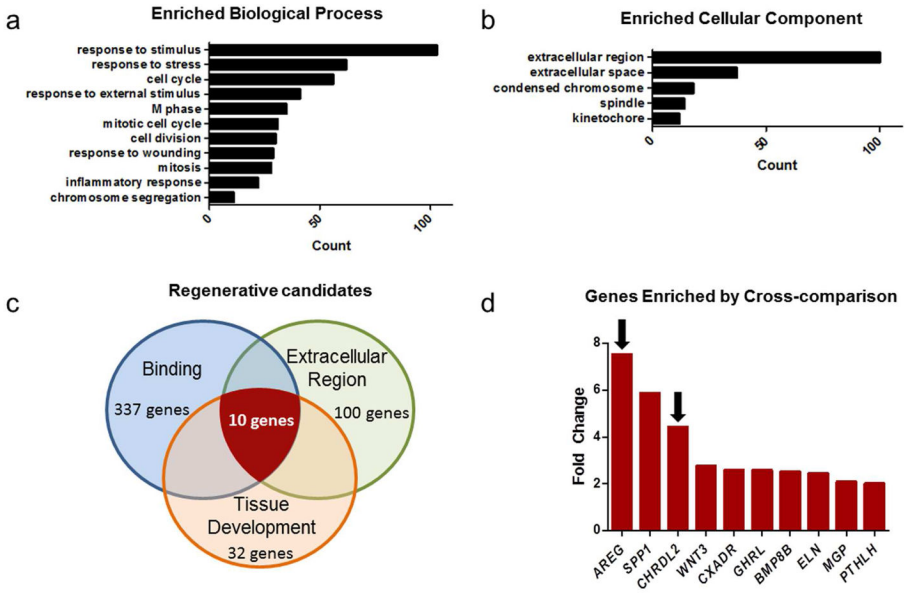

Fig. 6.

Gene Ontology (GO) analysis of sub-epithelial tissue (SET) microarray data. Panels **a** and **b** show the most abundant enriched categories within the biological properties and cellular component arms of GO. Panel **c** identifies regenerative candidates by cross comparison of relevant GO categories. Panel **d** shows the fold increase of the 10 transcripts identified in Panel **c** and arrows show the 2 secreted factors chosen to study with cultured crypts, i.e. amphiregulin and chordin-like 2.

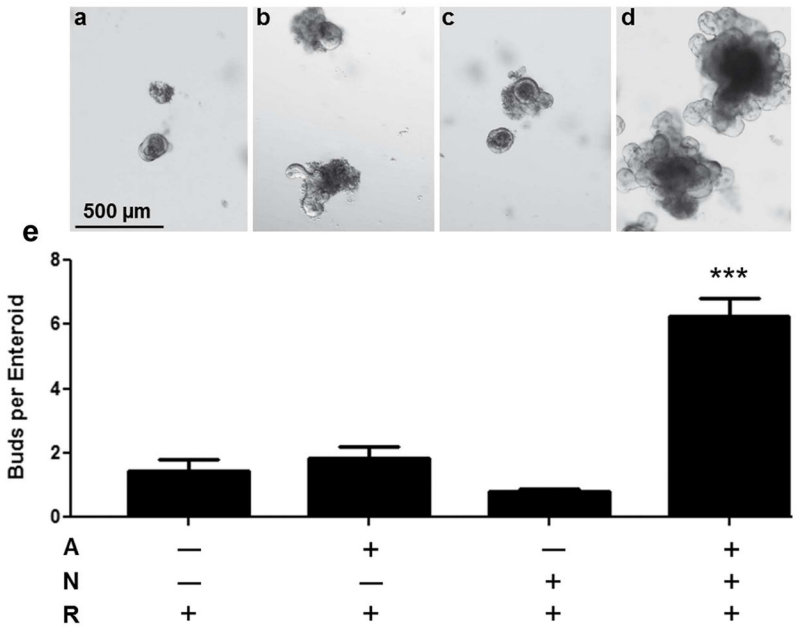

Fig. 7.

Effects of amphiregulin and BMP antagonism on crypts in culture. Control (untreated) crypts were grown for 7 days under minimal conditions established in Fig. 3 with: **a**: No added factors; **b**: amphiregulin (A) alone; **c**: Noggin (N) alone; and **d**: Both amphiregulin and noggin. Top panels show representative images with bars showing 500 μm and lower panel shows buds per enteroid as means ± SEM, n=5 per condition. ***$p<0.001$; compared with condition a.

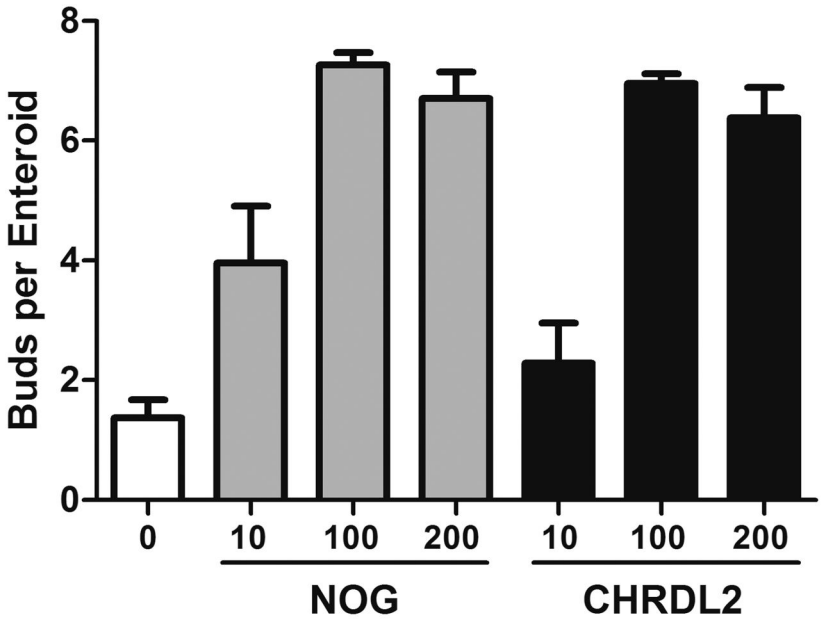

Fig. 8.

Dose response of chordin-like 2 in comparison with noggin on crypts in culture. Control crypts were grown for 7 days under minimal conditions established in Fig. 3 with added amphiregulin as in Fig. 7 and with various concentrations of either noggin (NOG) or chordin-like 2 (CHRDL2). Each panel shows buds per enteroid as means ± SEM, n=2. Two-way ANOVA showed a significant effect of dose ($p<0.001$); but no significant difference between noggin and chordin-like-2 ($p>0.1$) and no significant interaction ($p>0.4$)

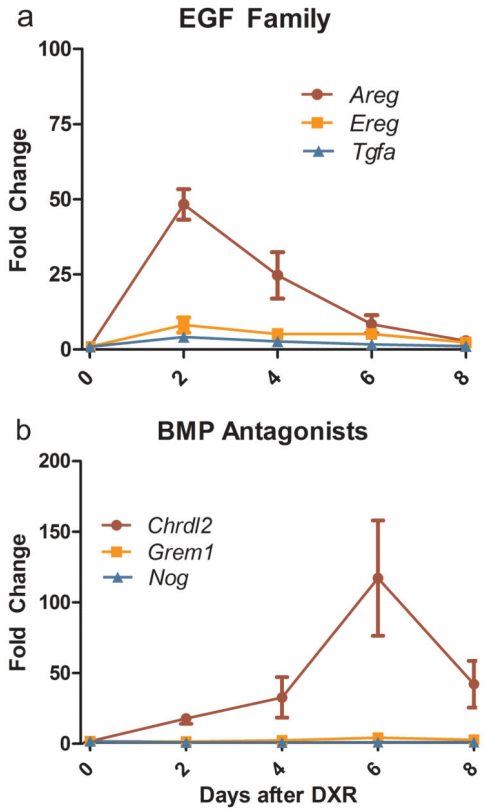

Fig. 9.

Quantitative RT-PCR analysis of RNA from SET harvested at 2, 4, 6, and 8 days following DXR administration for select EGF family members and BMP antagonists relative to untreated SET. a: EGF members shown include amphiregulin (Areg), epiregulin (Ereg), and transforming growth factor, alpha (Tgfa). b: Inhibitors of BMP analyzed include chordin-like 2 (Chrdl2), gremlin 1 (Grem1), and noggin (Nog). Bars show mean ± SEM, n = 3–5. All factors shown have $p < 0.05$ by one-way ANOVA.